Content

Table S1 Crystal data and structure refinement parameters of **1**.

Table S2 Selected bond lengths (Å) and angles (°) for **1**.

Table S3 Standard deviation and detection limit calculation for acetone, Fe^{3+} and Cu^{2+}.

Table S4 Standard deviation and detection limit calculation for $Cr_2O_7^{2-}$, CrO_4^{2-} and NZF.

Table S5 Comparison of various CPs sensors for the detection of acetone.

Table S6 Comparison of various CPs sensors for the detection of Fe^{3+} and Cu^{2+} ions.

Table S7 Comparison of various CPs sensors for the detection of $Cr_2O_7^{2-}$ and CrO_4^{2-} ions.

Table S8 Comparison of various CPs sensors for the detection of NFT.

Table S9 HOMO and LUMO energy levels of selected antibiotics and H_4L calculated by density functional theory (DFT) at $B_3LYP/6\text{-}31G^{**}$ level.

Scheme S1 Schematic drawing of the ligands H_4L and BIP.

Scheme S2 The coordination mode of L^{4-} ligand.

Scheme S3 The structures of selected antibiotics.

Figure S1 The IR spectra of **1**.

Figure S2 The 1D $[Zn(BIP)]_n$ chain in **1**.

Figure S3 The PXRD patterns of **1** before and after sensing tests.

Figure S4 The TG curve of **1**.

Figure S5 The solid state fluorescent emission spectra for **1**.

Figure S6 (a) Emission spectra of **1** dispersed different solvent; (b) Emission spectra of **1** with different mixed solvents added acetone.

Figure S7 UV-vis spectra of different solvent and the emission spectra of **1** in DMF solution.

Figure S8 UV-vis spectra of different metal cations and the emission spectra of **1** in DMF solution.

Figure S9 UV-vis spectra of different anions and the emission spectra of **1** in DMF solution.

Figure S10 (a) UV-vis spectra of different antibiotics and the emission spectra of **1** in DMF solution; (b) The HOMO and LUMO energy levels for different antibiotics.

Table S1 Crystal data and structure refinement parameters of **1**.

	1
Formula	$C_{42}H_{31}N_{11}O_{10}Zn_2$
Formula weight	980.56
Crystal system	Orthorhombic
Space group	*P bcn*
a (Å)	12.0157(13)
b (Å)	18.1093(19)
c (Å)	18.990(2)
α (º)	90
β (º)	90
γ (º)	90
Volume (Å^3)	4132.2(8)
Z	4
T (K)	296(2)
D_{calcd} (mg·m^{-3})	1.576
μ (mm^{-1})	1.235
R_{int}	0.0585
F(000)	2000
θ range (º)	$2.034 \leq \theta \leq 26.000$
Reflns. collected	41035
Data / restraints / parameters	4066 / 0 / 294
Goodness of fit on F^2	0.996
Final *R* indices [$I > 2\sigma(I)$]	$R_1 = 0.0470$, $wR_2 = 0.1281$
R indices (all data)	$R_1 = 0.0718$, $wR_2 = 0.1394$
Largest diff. peak and hole (e Å^{-3})	0.614 and -0.646

$R_1 = \Sigma| |F_o|-|F_c| |/\Sigma|F_o|$. $\omega R_2 = \Sigma[w(F_o^2-F_c^2)^2]/\Sigma[w(F_o^2)^2]^{1/2}$

Table S2 Selected bond lengths (Å) and angles (°) for **1**.

1			
Zn(1)-O(1)	1.935(3)	Zn(1)-O(4)^{ii}	1.930(3)
Zn(1)-N(1)	2.029(3)	Zn(1)-N(3)^{i}	1.997(3)
O(1)-Zn(1)-N(1)	94.97(12)	O(1)-Zn(1)-N(3)^{i}	107.15(14)
O(1)-Zn(1)-O(4)^{ii}	116.03(12)	N(1)-Zn(1)-N(3)^{i}	107.37(14)
N(1)-Zn(1)-O(4)^{ii}	113.50(13)	N(3)^{i}-Zn(1)-O(4)^{ii}	115.64(14)

Symmetry codes: i: 1/2+x, -1/2+y, 1/2–z; ii: 3/2–*x*, -1/2+*y*, *z*.

Table S3 Standard deviation and detection limit calculation for acetone, Fe^{3+} and Cu^{2+}.

	acetone	Fe^{3+}	Cu^{2+}
1	674.964623	676.910132	679.979652
2	674.713217	676.712265	679.571873
3	674.771354	677.099955	679.711342
4	674.572372	676.633277	679.791236
5	675.113253	677.094345	680.021875
Standard deviation (σ)	0.19066	0.1917	0.16753
Slope (m)	6.79×10^4	2.93×10^4	1.39×10^4
Detection limit (3σ/m)	8.42×10^{-6}	1.96×10^{-5}	3.62×10^{-5}

Table S4 Standard deviation and detection limit calculation for $Cr_2O_7^{2-}$, CrO_4^{2-} and NZF.

	$Cr_2O_7^{2-}$	CrO_4^{2-}	NZF
1	680.438512	687.891131	640.928032
2	680.417532	687.654376	641.072251
3	680.731543	687.982273	640.701342
4	680.271586	687.512145	640.691276
5	680.831653	687.992165	641.1921367
Standard deviation (σ)	0.20932	0.19095	0.19869
Slope (m)	2.84×10^{4}	1.87×10^{4}	1.59×10^{4}
Detection limit (3σ/m)	2.21×10^{-5}	3.06×10^{-5}	3.75×10^{-5}

Table S5 Comparison of various CPs sensors for the detection of acetone.

	Analyte	CPs-based fluorescent Materials	Quenching constant (K_{SV}, M^{-1})	Detection Limits (LOD)	Media	Ref
1	acetone	$[Cd_3(cpota)_2(phen)_3]_n \cdot 5nH_2O$	78 M^{-1}	1.57×10^{-4}M	H_2O	18(a)
2		$[Cd_3(L^1)_2(BTB)_2(H_2O)] \cdot DMF \cdot H_2O$	3.3146	0.122 vol%	CH_3CN	18(b)
3		$\{[Cd(pta)] \cdot H_2O)\}_n$	6.37×10^3 M^{-1}	0.0825 vol% (825 ppm)	H_2O	18(c)
4		$[Cd(L^1)(oba)] \cdot DMF$	1.169 M^{-1}		DMF	18(d)
5		$[Zn_2(L^1)_2(HBPT)_2] \cdot H_2O$	0.7006 M^{-1}			
6		$\{[Cd(bct)(tib)] \cdot H_2O \cdot DMF\}_n$	12.89 M^{-1}		H_2O	18(e)
7		$[Zn_5(L)_4(H_2tpim)_2(FA)_4(H_2O)_2]_n$	3.948 mM^{-1}		DMF	18(f)
8		$[Zn(L)(Htpim)]_n$	3.138 mM^{-1}			
9		$[Zn(L)\ (Htpim)]_n$	1.731 mM^{-1}			
10		$\{[Cd(H_2O)_4(4\text{-}BPDB)][BPDC]\}_n$	13.57 M^{-1}	0.15 mM	CH_3CN	18(g)
11		$[Zn(L)(bpdc)] \cdot 1.6H_2O$	0.4788	0.0478 vol%	DMF	18(h)
12		$[Cd_2(L)(Hbptc)_2]$	0.4918	0.0465 vol%		
13		$[Zn_2(H_2BCA)_2(o\text{-}bimb)_2(H_2O)_2]_n$	3.7×10^4 M^{-1}	0.09 μM	H_2O	18(i)
14		$\{[Zn(H_2BCA)(m\text{-}bib)] \cdot H_2O\}_n$	2.0×10^4 M^{-1}	0.13 μM		

H_3cpota = 2-(4-carboxyphenoxy)terephthalic acid, phen = 1,10-phenanthroline; L^1=1, 3-di(1H-imidazol-4-yl)benzene, H_3BTB=1,3,5-tri(4-carboxyphenyl)benzene; H_2pta = 2-(4-pyridyl)-terephthalic acid; L^1=1,3-di(1H-imidazol-4-yl)benzene, H_2oba = 4,4′-oxybis-(benzoic acid), H_4BPTC = biphenyl-3,3′,5,5′-tetracarboxylic acid; H_2bct=3,5-bis(4′-carboxyphenyl)-1,2,4-triazole, tib = 1,3,5-tris(1-imidazolyl)benzene; H_2L=5-nitroisophthalic acid, Htpim=2,4,5-triIJ4-pyridyl)-imidazole, HFA = formic acid; 4-BPDB=1,4-bis(4-pyridyl)-2,3-diaza-1,3-butadiene, H_2BPDC=4,4′-biphenyldicarboxylic acid;

H_2bpdc =4,4′-benzophenonedicaboxylic acid, H_3bptc = biphenyl-2,4′,5-tricarboxylic acid, L=1,4-di(1H-imidazol-4-yl)benzene;

H_2BCA=bis(4-carboxybenzyl)amine, o-bimb = 1,2-bis(imidazol-1-ylmethyl) benzene), m-bib = 1,3-bis(1-imidazoly)benzene.

Table S6 Comparison of various CPs sensors for the detection of Fe^{3+} and Cu^{2+} ions.

	Analyte	CPs-based fluorescent Materials	Quenching constant (K_{SV}, M^{-1})	Detection Limits (LOD)	Media	Ref
1	Fe^{2+}	$[Mg_2(APDA)_2(H_2O)_3]\cdot 5DMA\cdot 5H_2O$	2.06×10^4	152 ppb	DMF	19(a)
2		$\{Eu_2L_3(DMF)\}\cdot 2DMF$	4×10^4	6.62 μM	H_2O	19(b)
3		$[Ag(CIP^-)]$	7.1×10^3	1.2×10^{-6} M	H_2O	19(c)
4		$[Zn(ACA)_4]\cdot CB[6]\cdot [NH_2(CH_3)_2]\cdot 8H_2O$	1.088×10^4	9.5×10^{-7} M	H_2O	19(d)
5		$\{[Eu_2(L)_2(H_2O)_2]\cdot 5H_2O\cdot 6DMAC\}_n$	5941 M	10^{-5} mM	H_2O	19(e)
6		$[Ln_2(L^1)_2(H_2O)_4]\cdot 2H_2O$		10^{-6} M	H_2O	19(f)
7		$[Tb(HMDIA)(H_2O)_3]\cdot H_2O$	1.6×10^4 M^{-1}		H_2O	19(g)
1	Cu^{2+}	$\{[BaCd(\mu_6\text{-tp})_{1.5}(\mu_2\text{-Cl})(H_2O)(DMF)_2]\cdot 0.75H_2O\}_n$	1.15×10^4 M^{-1}	0.26 μM	H_2O	20(a)
2		$\{Cd(INA)(pytpy)(OH)\cdot 2H_2O\}_n$	1.3×10^5 M^{-1}	3.98×10^{-3} mM	H_2O	20(b)
3		$[Cd(L)]\cdot 2DMF$	4.1×10^3 M^{-1}		DMF	20(c)
4		$\{[Zn(btca)(py)_2]\}_n$	2.92×10^4 M^{-1}	3 ppm	H_2O	20(d)
5		$\{Eu_2(TBrTA)_3(H_2O)_8\cdot 2H_2O\}_n$	4612.0 M^{-1}	7.52×10^{-5} mol/L	ethanol	20(e)
6		$\{[Ln_3Ag_3(BPDC)_5(OX)(H_2O)_7]\cdot 7H_2O\}_n$	4674 M^{-1}		ethanol	20(f)
7		$Cd_2(dhtp)(DMF)_2$	1806 M^{-1}		H_2O	20(g)
8		$[Cd(L)(TPOM)_{0.75}]\cdot xS$	17890 M^{-1}		H_2O	20(h)

H_2APDA= 4,4′-(4-aminopyridine-3,5-diyl)dibenzoic acid;

L=(6-[1-(4-carboxyphenyl)-1H-1,2,3-triazol-4-yl]nicotinic acid;

HCIP = 4-(4-carboxylphenyl)-2,6-di(4-imidazol-1-yl)phenyl)pyridine;

CB[6]=cucurbit[6]uril, HACA = anthracene-9-carboxylic acid;

H_3L = 4,4'-(((5-carboxy-1,3-phenylene)bis(azanediyl))bis(carbonyl)) dibenzoic acid, DMAC = N,N'-dimethylacetamide;

H_4MDIA=5,5′-methylenediisophthalic acid;

H_2tp = terephthalic acid;

pytpy = 4′-(4-Pyridinyl)-2,2′:6′,2”-terpyridine, INA = Isonicotinic acid;

L= 5,5′,5"-((1,3,5-triazine-2,4,6-triyl)tris(azanediyl))tris(3-methylbenzoic acid);

H_2btca = benzotriazole-5-carboxylic acid, py = pyridine;

H_2TBrTA= tetrabromoterephthalic acid;

H_2BPDC=2,2’-bipyridine-3,3’-dicarboxylic acid, H_2OX= oxalic acid; H_2dhtp =2,5-dihydroxy-1,4-benzenedicarboxylic acid;

TPOM = tetrakis(4-pyridyloxy-methylene) methane.

Table S7 Comparison of various CPs sensors for the detection of $Cr_2O_7^{2-}$ and CrO_4^{2-} ions.

	Analyte	CPs-based fluorescent Materials	Quenching constant (K_{SV}, M^{-1})	Detection Limits (DL)	Media	Ref
1	$Cr_2O_7^{2-}$	$[H_2N(CH_3)_2]_2[Zn_2L(HPO_3)_2]$	4.44×10^4	1.09×10^{-3} mM	H_2O	20(a)
2		$[Tb(ppda)(bdc)_{0.5}(C_2H_5OH)(H_2O)]_n$	4.03×10^3	5.0×10^{-5} M	DMF	20(b)
3		$\{[(CH_3)_2NH_2]_2$ $[Zn_5$ $(TDA)_4TZ)_4]$ □4DMF$\}_n$	6.77×10^3	7.48 μmol L^{-1}	H_2O	20(c)
4		$[Cd_3(cpota)_2(phen)_3]_n \cdot 5nH_2O$	1.21×10^4	3.70×10^{-7} M	H_2O	20(d)
5		$[Zn(NH_2\text{-}bdc)(4,4'\text{-}bpy)]$	7.62×10^3	1.30 μM	H_2O	20(e)
6		$\{[Cd_2L_2(H_2O)_4] \cdot H_2O\}_n$	1.25×10^4	3.7 μM	H_2O	20(f)
7		$\{[Zn_2L_2(H_2O)_4] \cdot H_2O\}_n$	1.77×10^4	2.6 μM	H_2O	
1	CrO_4^{2-}	$[Cd_{1.5}(L)_2(bpy)(NO_3)] \cdot 2DMF \cdot 2H_2O$	1.73×10^4	280 ppb	H_2O	21(a)
2		$[Zn_2(TPOM)(NDC)_2] \cdot 3.5H_2O$	7.81×10^3	2.50 μM	H_2O	21(b)
3		$\{[Zn(L)_{0.5}(bimb)] \cdot 2H_2O \cdot 0.5(CH_3)_2NH\}_n$	5.04×10^4	0.60 μM	H_2O	21(c)
4		[Ni(ppvppa)(5-NO_2-1,3-BDC)(H_2O)]· 0.5MeCN	210526	0.09 ppb	H_2O	21(d)
5		$\{[Cd_2L_2(H_2O)_4] \cdot H_2O\}_n$	1.21×10^4	3.8 μM	H_2O	21(e)
6		$\{[Zn_2L_2(H_2O)_4] \cdot H_2O\}_n$	1.95×10^4	2.3 μM		
7		$[Eu_7(mtb)_5(H_2O)_{16}] \cdot NO_3 \cdot 8DMA \cdot 18H_2O$	3.3×10^4		H_2O	21(f)

H_2L=2′,3′,5′,6′-tetramethyl-[1,1′:4′,1″-terphenyl]-4,4″-dicarboxylic acid;

H_2ppda=4-(pyridin-3-yloxy)-phthalic acid, H_2bdc=terephthalic acid;

H_2TDA = thiophene-2,5-dicarboxylic acid, HTZ = 1H-1,2,4-Triazole;

H_3cpota = 2-(4-carboxyphenoxy)terephthalic acid, phen = 1,10-phenanthroline;

NH_2-H_2bdc = 2-amino-1,4-benzenedicarboxylic acid, 4,4'-bpy = 4,4'-bipyridine;

H_2L = 5-(1H-1,2,4-triazol-1-yl)isophthalic acid);

HL = 4-(4-carboxyphenyl)-1,2,4-triazole, bpy = 4,4′-bipyridine;

TPOM = tetrakis(4-pyridyloxymethylene)methane, H_2ndc = 2,6-naphthalenedicarboxylic acid;

ppvppa = dipyridin-2-yl-[4-(2-pyridin-4-yl-vinyl)-phenyl]-amine, 5-NO_2-1,3-H_2BDC = 5-nitroisophthalic acid.

H_2L = 5-(1H-1,2,4-triazol-1-yl)isophthalic acid;

H_4mtb = 4-[tris(4-carboxyphenyl)methyl]benzoic acid.

Table S8 Comparison of various CPs sensors for the detection of NFT.

	Analyte	CPs-based fluorescent Materials	Quenching constant (K_{SV}, M^{-1})	Detection Limits (LOD)	Media	Ref
1	NFT	$\{[Cd_3(TDCPB)\cdot 2DMAc]\cdot DMAc\cdot 4H_2O\}_n$	1.05×10^5		DMA	22(a)
2		$\{[Tb(TATMA)(H_2O)\cdot 2H_2O\}_n$	3.35×10^4		H_2O	22(b)
3		$[Zn(L)_2]\cdot CH_2Cl_2\cdot CH_3OH$	1.58×10^4		CH_3OH	22(c)
4		$[Cd(tptc)_{0.5}(o\text{-}bimb)]_n$	3.4×10^4		DMF	22(d)
5		$[Cd(H_2tptc)_{0.5}(mbimb)(Cl)]_n$	2.6×10^5		DMF	
6		$[TbL\cdot 2H_2O]_n$	5.26×10^4		H_2O	22(e)
7		$[Zn_2(azdc)_2(dpta)]\cdot(DMF)_4$	7.14×10^4		DMF	22(f)

TADA = 3,3′-((6-hydroxy-1,3,5-triazine-2,4-diyl)bis(azanediyl))dibenzoate;

H_3L = 4-(2,4,6-tricarboxyl phenyl)-2,2′:6′,2″- terpyridine;

H_3L = 5-(4-carboxy-phenoxymethyl)-isophthalic acid;

H_2NDC= 1,4-naphthalenedicarboxylic acid;

H_3TATMA= 4, 4′,4″-s-triazine-1,3,5-triyltri-m-aminobenzoate.

Table S9 HOMO and LUMO energy levels of selected antibiotics and H_4L calculated by density functional theory (DFT) at $B_3LYP/6\text{-}31G^{**}$ level.

	HOMO (eV)	**LUMO (eV)**	**Band Gap (eV)**
NFT	-6.70	-3.12	3.58
DTZ	-6.93	-2.32	4.61
SDZ	-6.20	-1.02	5.18
CAP	-7.24	-2.52	4.72
PCL	-6.49	-0.50	5.99
H_4L	-6.88	-2.53	4.35

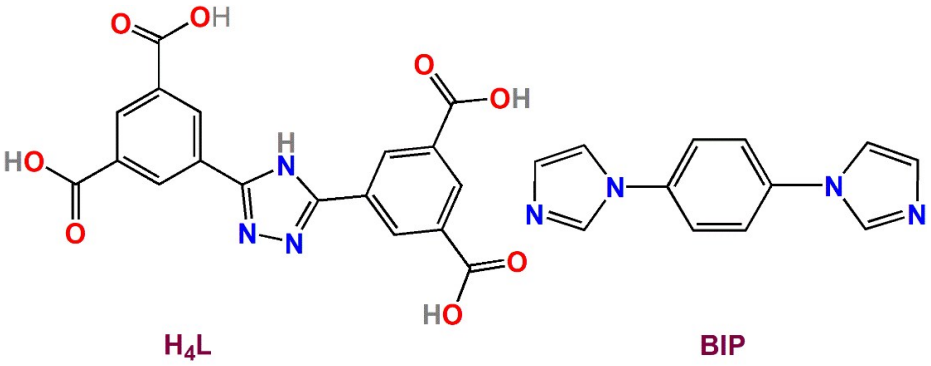

Scheme S1 Schematic drawing of the ligands H_4L and BIP.

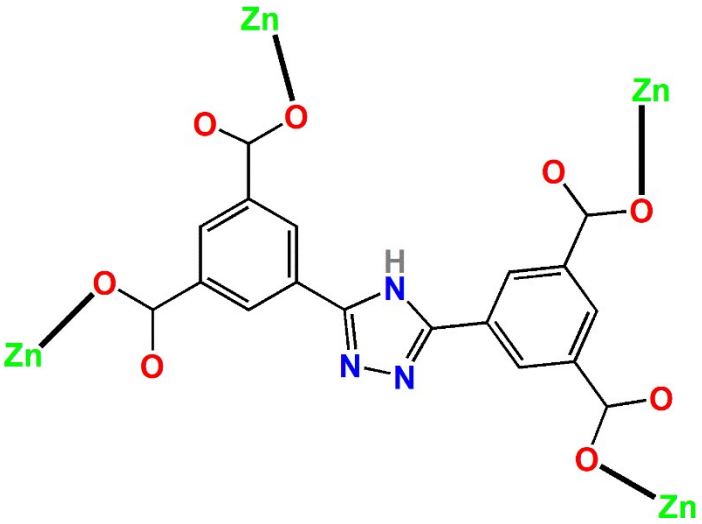

Scheme S2 The coordination mode of L^{4-} ligand.

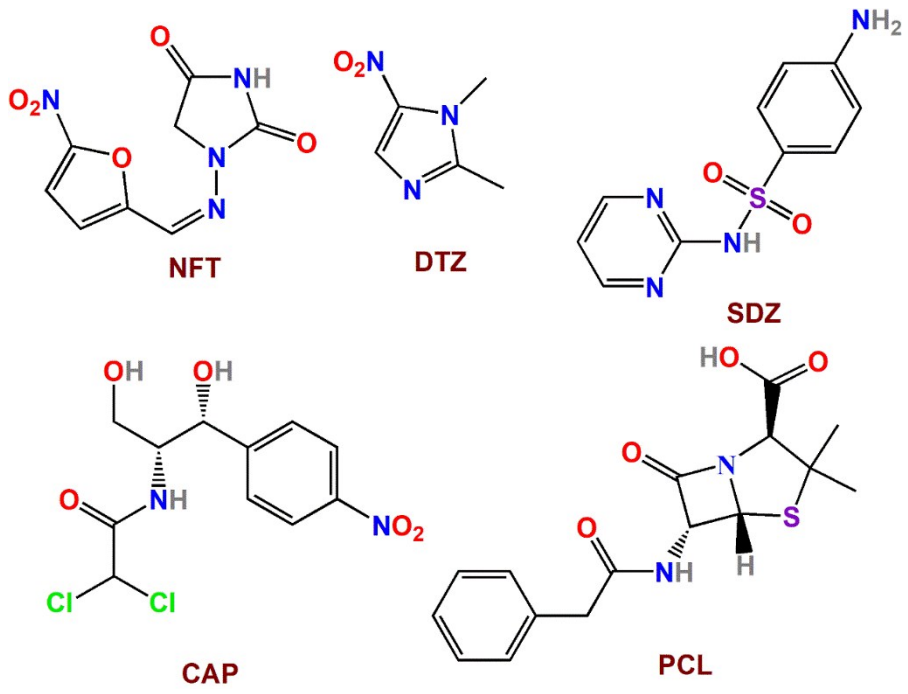

Scheme S3 The structures of selected antibiotics.

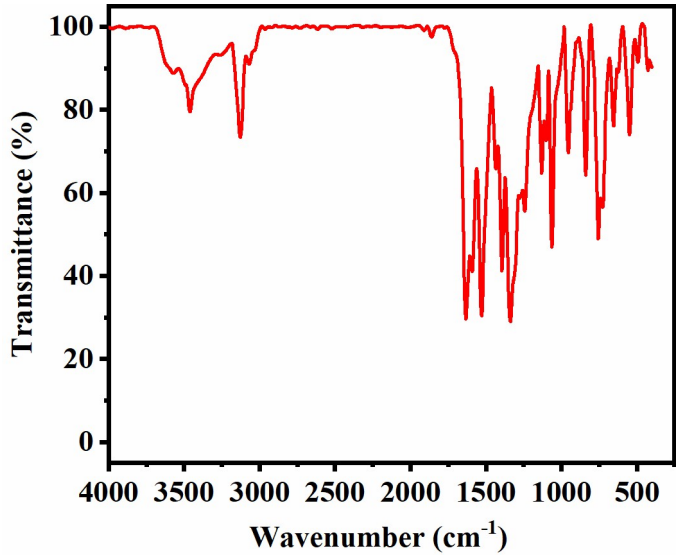

Figure S1 The IR spectra of **1**.

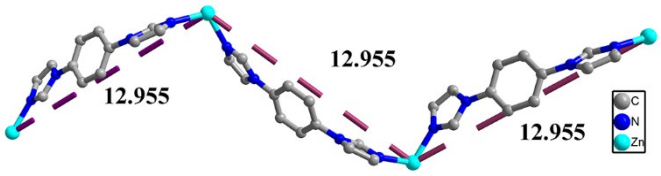

Figure S2 The 1D $[Zn(BIP)]_n$ chain in **1**.

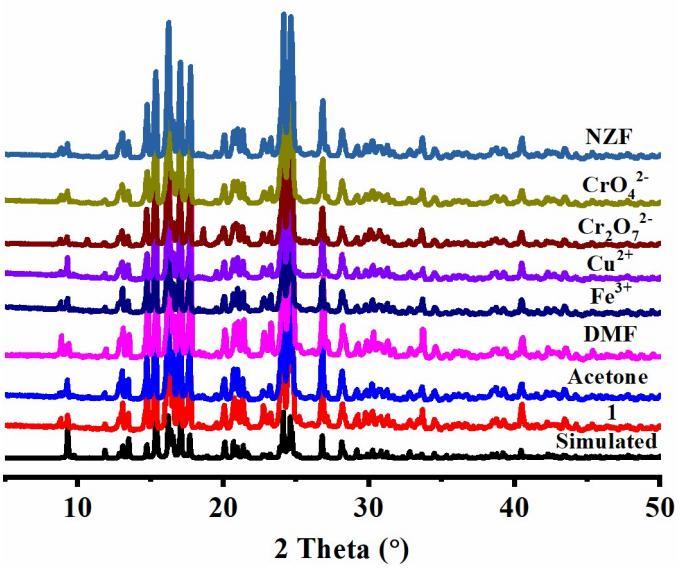

Figure S3 The PXRD patterns of **1** before and after sensing tests.

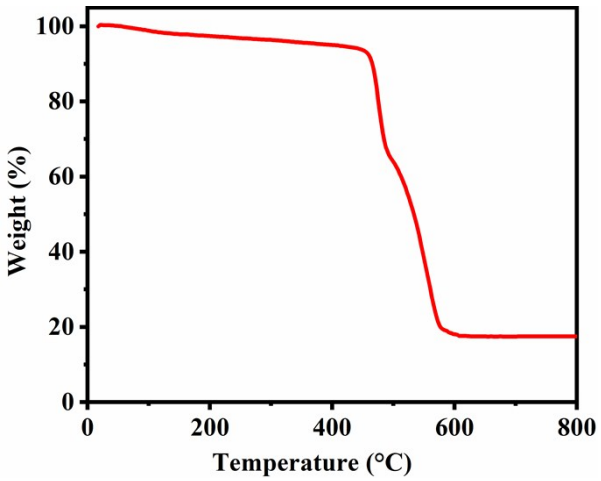

Figure S4 The TG curve of **1**.

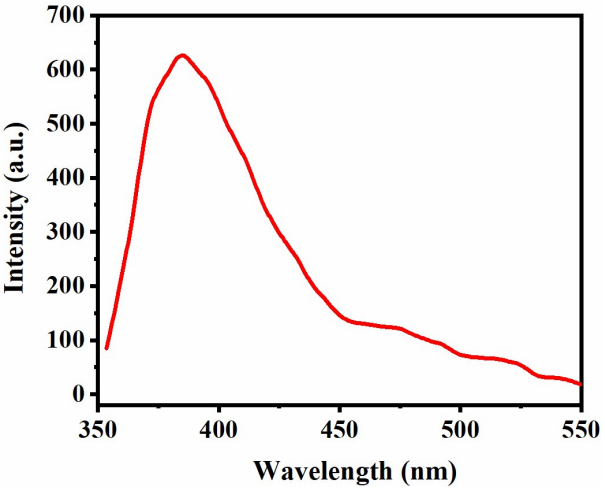

Figure S5 The solid state fluorescent emission spectra for **1**.

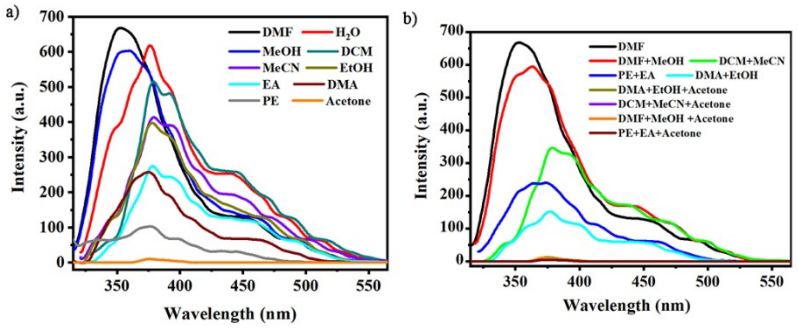

Figure S6 (a) Emission spectra of **1** dispersed different solvent; (b) Emission spectra of **1** with different mixed solvents added acetone.

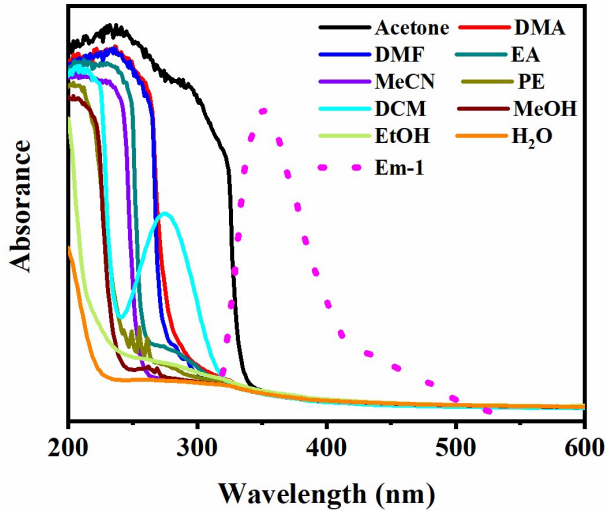

Figure S7 UV-vis spectra of different solvent and the emission spectra of **1** in DMF solution.

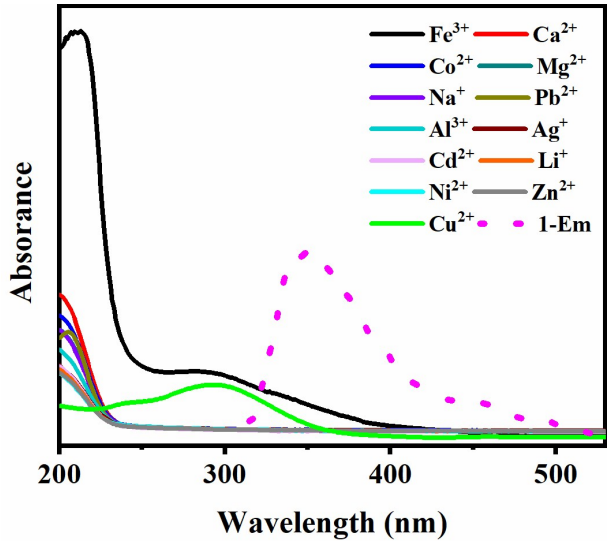

Figure S8 UV-vis spectra of different metal cations and the emission spectra of **1** in DMF solution.

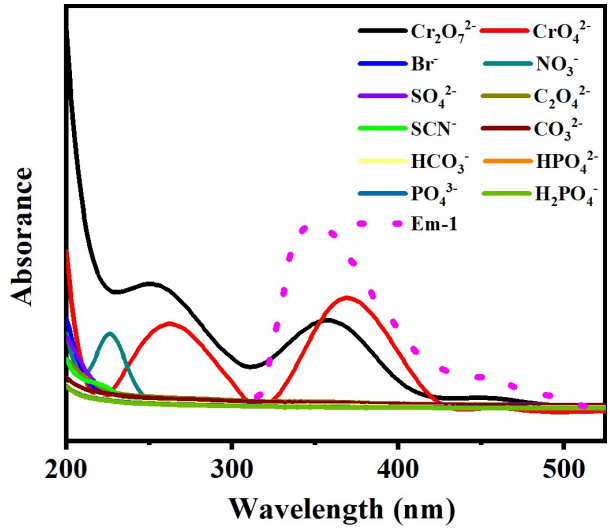

Figure S9 UV-vis spectra of different anions and the emission spectra of **1** in DMF solution.

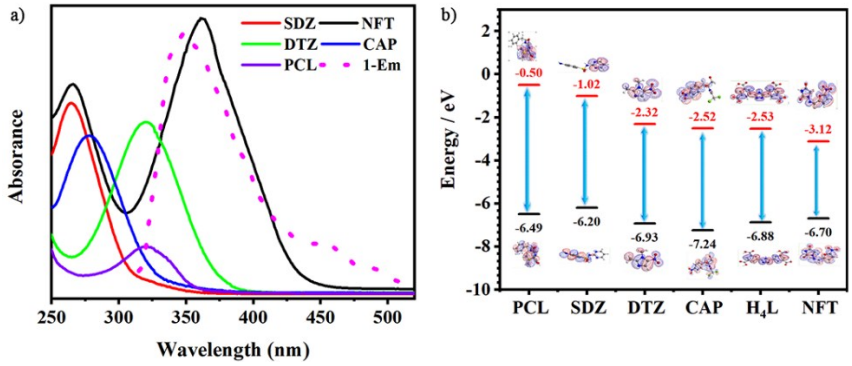

Figure S10 (a) UV-vis spectra of different antibiotics and the emission spectra of **1** in DMF solution; (b) The HOMO and LUMO energy levels for different antibiotics.